Acta Cryst. (1995). B**51**, 580–591

Experimental Evidence for the Existence of Non-nuclear Maxima in the Electron-Density Distribution of Metallic Beryllium. A Comparative Study of the Maximum Entropy Method and the Multipole Refinement Method

BY BO BRUMMERSTEDT IVERSEN AND FINN KREBS LARSEN†

Department of Chemistry, Aarhus University, DK 8000 Aarhus C, Denmark

MOHAMMED SOUHASSOU‡

Medical Foundation of Buffalo, Buffalo, NY 14214, USA

AND MASAKI TAKATA

Department of Applied Physics, Nagoya University, Nagoya 464-01, Japan

(*Received* 9 *May* 1994; *accepted* 12 *September* 1994)

Abstract

The electron-density distribution (EDD) of metallic beryllium has been derived from the structure factors of Larsen & Hansen [(1984). *Acta Cryst.* B**40**, 169–179] using the maximum entropy method (MEM). Subsequent topological analysis reveals non-nuclear maxima (NNM) in the EDD. Plots of the gradient field of the electron density illustrates this finding. A possible critical-point network for the hexagonal close-packed (h.c.p.) structure of beryllium is suggested. It is thus demonstrated that it is possible to obtain detailed topological information about the electron density in metallic beryllium without the use of a structural model. In order to test the findings of the MEM, the same set of structure factors were analysed using the multipole refinement method (MRM). Use of the MRM also reveals NNM. The results of the two different approaches to electron-density analysis are contrasted and discussed. Expressed within the framework of the theory of atoms in molecules, our results suggest that the h.c.p. structure of beryllium has no Be atoms directly bonded to other Be atoms. The structure is held together through a three-dimensional network of bonds between the NNM and Be atoms as well as between different NNM. The topological analysis thus reveals that the beryllium structure has important interactions connecting Be atoms of different basal plane layers. The breaking of these interactions when forming a surface may explain the abnormally large expansion of the inter-layer distance in the beryllium surface structure.

Introduction

Numerous theoretical calculations by varying techniques have derived the electron-density distribution (EDD) of different metals and these have been compared with state-of-the art experimental determinations. Theoretical reports have shown (Cao, Gatti, Macdougall & Bader, 1987; Edgecombe, Smith & Muller-Plathe, 1993) that non-nuclear maxima may exist in simple metals. This is a most interesting result because a dominant feature in molecular electron-density distributions is that they exhibit maxima only at the nuclear positions (Bader, 1991).

From cluster calculations on lithium and sodium, Cao, Gatti, Macdougall & Bader (1987) found that the alkali metals consist of positively charged metal ions immersed in and bound through an inter-meshed network of negative charge concentrations, so called non-nuclear attractors or non-nuclear maxima (the NNM). Later Edgecombe, Smith & Muller-Plathe (1993) have shown that the NNM in sodium were artifacts of the basis set used in the calculation, but that the NNM in lithium were persistent. The NNM consist of loosely bound and quite delocalized electronic charge and so must be important for the metallic conducting properties. It is thus of interest to characterize further the possible NNM in metals. Beryllium is most suitable for performing high-resolution X-ray diffraction experiments. The crystal data for beryllium are: space group $P6_3/mmc$, Z = 2, a = 2.2853 (3), c = 3.5842 (2) Å at T = 293 K. Because of its low atomic number and the availability of high-quality crystals, minimal systematic errors are encountered in the data collection. For this reason beryllium was chosen as a test for checking whether the theoretical findings may be a more general feature of metallic systems. Earlier experimental work on metallic beryllium by Larsen & Hansen (1984) has shown an accumulation of charge in the bipyramidal space of tetrahedral holes in the h.c.p. structure. That work was a combined X-ray, neutron and γ-ray diffraction experiment. Using Fourier summation techniques Larsen and Hansen found a surplus of 0.013 (2) electrons in

† Author to whom correspondence should be addressed.

‡ Present address: Laboratoire de Minéralogie-Cristallographie, Université de Nancy I, BP 239, 54506 Vandoeuvre CEDEX, France.

the bipyramidal space relative to a free atom model. Theoretical *ab initio* LCAO calculations by Dovesi, Pisani, Ricca & Roetti (1982) also suggested a NNM at the midpoint of the bipyramidal space of tetrahedral holes. Chou, Lam & Cohen (1983) performed *ab initio* local density functional calculations. Their calculations indicated small NNM but in another position than found by Dovesi, Pisani, Ricca & Roetti (1982). *Ab initio* Hartree–Fock–Rothan cluster calculations by Ross, Ermler, Kern & Pitzler (1992) also indicate the existence of NNM. Very recently, Holzwarth & Zeng (1994) performed local density functional calculations which show a peak at the midpoint of the bipyramidal space both in the valence charge density and in the deformation density.

In the present paper we report a topological analysis of the experimental charge density of beryllium derived using the structure factors of Larsen & Hansen (1984) by both the maximum entropy method (MEM) (Collins, 1982; Sakata & Sato, 1990) and the multipole refinement method (MRM) (Stewart, 1976; Hansen & Coppens, 1978). The derived electron densities were analysed using the FORTRAN program *CPGRID* for the MEM case and the program *POTLAPDENS* in the MRM case (Souhassou, 1993). The results obtained with the two different methods are contrasted and virtues as well as drawbacks of the methods are discussed.

The maximum entropy method

The strong point of the MEM used for data analysis is that it uses the full Bayes' equation (1) and introduces the prior probability distribution in the inference of the EDD (Skilling, 1991; Smith & Erickson, 1989).

$$P(\text{model/data}) = P(\text{data/model}) \times P(\text{model})/P(\text{data}) \quad (1)$$

In this expression P(data/model) is the likelihood function. If the error distribution is known around each data point the likelihood function is a computable distribution. Conventional least-squares refinement corresponds in the case of Gaussian error distributions to maximizing the likelihood function. However, the likelihood function is not equal to P(model/data), the posterior distribution, which is the distribution we want to know. From Bayes' equation, (1), it can be seen that least-squares analysis corresponds to the omission of the factor P(model)/P(Data). P(Data) can be taken as a constant but P(model), the prior probability distribution, in general cannot. The prior probability distribution is of little consequence when we are dealing with good and abundant data, but it is an important factor when dealing with limited or poor data sets. In a diffraction experiment the number of structure factors measurable is eventually limited by the maximum length of the scattering vector ($4\pi/\lambda$). In practice the upper limit is considerably lower. In experimental electron-density analysis one tries to extrapolate the resolution of the EDD to infinity from this limited number of structure factors. This is an underdetermined system and therefore an infinity of different EDD's will have identical misfit statistics. In this case it is important to include the prior probability distribution in the inference of the density. It has been shown that for positive and additive distributions the prior distribution takes on an entropic functional form (Skilling, 1989). The most unbiased inference one can make is, therefore, to choose the density that maximizes the entropy and at the same time fulfils the constraint of the data.

The maximum entropy method can be introduced in electron-density determination by an iteration procedure. The unit cell is divided into a number of pixels. Within the approximations suggested by Collins (1982) and Sakata & Sato (1990) the normalized density ρ_x, in pixel number x, can be calculated in an iterative manner from the normalized density in the previous cycle, τ_x, by the expression

$$\rho_x = \exp\{\ln\tau_x + F_0\lambda/N\Sigma[(F_{\mathbf{H}}^O - F_{\mathbf{H}}^C)/\sigma_{\mathbf{H}}^2]\exp(-2\pi i\mathbf{H}x)\}. \quad (2)$$

In this formula F_0 is the number of electrons in the unit cell and λ is a Lagrangian multiplier. $F_{\mathbf{H}}^O$ are the experimentally observed structure factors and $F_{\mathbf{H}}^C$ the calculated structure factors obtained as the Fourier summation of the unit-cell density. τ_x is a prior distribution which may contain our information about the system before performing the experiment. In the procedure used so far the iterations are stopped when the constraint $C_1 = 1/N\Sigma|F_{\mathbf{H}}^O - F_{\mathbf{H}}^C|^2/\sigma_{\mathbf{H}}^2$ has converged to a value of 1. N is the number of structure factors used in the analysis. This expected value of the constraint is based on the assumption that we can assign correct standard deviations to our experimentally measured structure factors. Gull (1989) has pointed out that this may not be the best way to solve the problem.

In the formalism above a prior distribution τ_x is introduced. The optimization procedure is dependent on the particular choice of this distribution. The straightforward possibility for introduction of all the prior knowledge one may have about the system being studied is a virtue of the MEM. The prior distribution allows us to incorporate information from earlier experiments or other sources. The optimization minimizes the cross entropy with respect to the prior model while fitting the data (Kapur & Kesavan, 1992). If we do not measure new data that contradict our prior knowledge then the resulting distribution will be the prior distribution. There is a conceptual difference between maximizing the entropy, $\rho_i\ln\rho_i$, under the constraints of the data (MaxEnt) and minimizing the cross entropy with respect to a prior distribution under the constraints of the data (MinXEnt) (Kapur & Kesavan, 1992). In the former case one wishes to maximize the entropy (uncertainty) of the distribution and thus make the most unbiased inference about the posterior distribution. In the latter case the basic concept

is minimization of the distance to the prior distribution. If a uniform prior distribution is chosen in MinXEnt then the two approaches are identical.

The multipole refinement method

In normal crystallographic work a model is suggested and the description of the EDD is parameterized and refined in a least-squares procedure minimizing the quantity $\Sigma w(|F_{\mathbf{H}}^{O} - kF_{\mathbf{H}}^{C}|^2)$, where $w = 1/\sigma^2(F_{\mathbf{H}}^2)$ and k is a scale factor. In most applications atom-centred model functions are used. In the model proposed by Hansen & Coppens (1978) the Fourier transform of the sum of atomic density contributions (3) is fitted to the observed structure factors

$$\rho_{\text{atom}} = P_{\text{core}}(r)\rho_{\text{core}} + P_{\text{val}}(r)\kappa^3\rho_{\text{val}}(\kappa r) + \sum_{l=0}^{l\max} \kappa'^3 R_l(\kappa' r) \sum_{m=0}^{l} P_{lm\pm} d_{lm\pm}(\theta,\varphi). \quad (3)$$

The use of nuclear centred model functions may conceivably have problems in describing very weak non-nuclear maxima. This is because the particular choice of model used in the least-squares fit inevitably will bias the resulting EDD. Differentiation between models that have the same residual is based either on chemical intuition or comparison with other experimental or theoretical results. A great amount of work has been devoted to finding out what type of functions give the physically most sensible EDD's after a least-squares refinement. In recent years it has become evident that also the shape of the radial functions used in the least-squares procedure can have a great influence on the final result (Figgis, Iversen, Larsen & Reynolds, 1993). Even though such bias is unsatisfactory, a great virtue of the method is that the electron density is parametrized into analytical functions. For molecular crystals this is generally carried out with great efficiency. The parametrization makes further analysis more convenient and allows physical properties to be calculated and compared with results of other experiments or calculations. (*e.g. d*-orbital populations, electrostatic properties *etc.*). However, the choice of model is not always obvious and it is very often seen that the parameters found in a least-squares analysis are highly correlated and therefore their individual numerical values are of little use. The theory of atoms in molecules (Bader, 1991) has provided experimental EDD analysis with a framework in which representations of the total EDD can also be analysed in a rewarding manner. A complication when performing a multipole analysis of metallic beryllium is that the EDD of a metal is very delocalized and therefore a very flexible model may be needed to describe the density. Extra flexibility can be obtained by using higher than fourth-order multipoles, which has been tried by Stewart (1977). However, a satisfactory model was obtained within the limitations of fourth-order multipoles.

A final point in favour of the MRM is that within the convolution approximation it gives parameters describing a static electron density. This is in contrast to the MEM which in the present form obtains the thermally smeared EDD. Static electron-density distributions can be directly compared to theoretically derived distributions, whereas thermally smeared distributions cannot.

Topological analysis of charge densities

Topological analysis of electron densities has been extensively presented in the literature, see for instance the book by Bader (1991). Critical points in the density have $\nabla\rho = 0$ and they can in Bader's scheme be classified in terms of the properties of the eigenvalues of the Hessian matrix (second derivatives) at the critical point. The critical points are characterized by (rank, signature), where rank is the number of non-zero eigenvalues and signature is the algebraic sum of their signs. Atomic entities in the density are (3,–3) points (also called peaks) and chemical bonds are (3,–1) points (passes). (3,1) and (3,3) points defines the two other structural units namely rings (pales) and cages (pits). The names in parenthesis were introduced by Johnson (1992). A very important theorem in the theory of atom in molecules connects the Laplacian of the density with the energy densities, $16m\pi^2\nabla^2\rho(\mathbf{r}) = 2G(\mathbf{r}) + V(\mathbf{r})$. $G(\mathbf{r})$ is the kinetic energy density and $V(\mathbf{r})$ is the potential energy density. On this basis, different bonds can be characterized depending on the sign of the Laplacian at the bond critical point. Closed-shell interactions have positive Laplacians (hydrogen bonds, van der Waal bonds *etc.*), whereas shared interactions have negative Laplacians (covalent bond). The π-character as well as the stability of a bond can be described by the ellipticity of the bond, $\varepsilon = \lambda_1/\lambda_2 - 1$, where λ_1 and λ_2 are the negative eigenvalues of the Hessian matrix at the bond critical point.

In recent years several reports (Stewart, 1991) have shown that valuable physical and chemical information can be obtained from topological methods applied to experimentally derived EDD's. Consequently there is a strong need to construct the optimum density based on the available information. When carrying out a topological analysis on an EDD one looks for not only the coarse features (the atomic maxima), but all the critical points in the structure. As will be shown two EDD's can have almost identical misfit statistics but still be different. Thus, it may be difficult in experimental EDD analysis to decide unambiguously which critical points are correct.

Calculations

The MEM formalism sketched above has been implemented in the program *MEED* from Nagoya University (Kumazawa, Kubota, Takata, Sakata & Ishibashi, 1993). In the present analysis 58 structure factors with $\sin\theta/\lambda \leq$

1.21 Å^{-1} measured by Larsen & Hansen (1984) were used. The MEM density was calculated on a 120 × 120 × 120 pixel grid (0.038 × 0.038 × 0.06 Å) for the final results. Exploratory calculations were done on a 60 × 60 × 60 pixel grid. Major topological features did not depend on the number of grid points indicating that the grid was chosen with adequate resolution. Initial calculations were started from a flat uniform distribution constrained to eight electrons in the unit cell. The Lagrangian multiplier was chosen small to ensure convergence. Iterations were stopped when the constraint C_1 had converged to a value of 1. This final density gave a residual factor, $R = \Sigma|F_H^O - F_H^C|^2/\Sigma|F_H^O|^2 = 0.006$. In Figs. 1(*a*) and 1(*b*) the resulting MEM electron density distribution in the basal plane (001) and in the (110) plane is shown. The contour lines are drawn in linear scale and only in the lower density region in order to better show the modulation of the EDD in the interatomic region. No absolute stopping criteria for the iterations exist in the present formalism. Densities were also calculated with constraint values, C_1, of 10, 5, 2, 0.75, 0.5, 0.25, 0.1 and 0.001, and the stability of the features in the maps was confirmed.

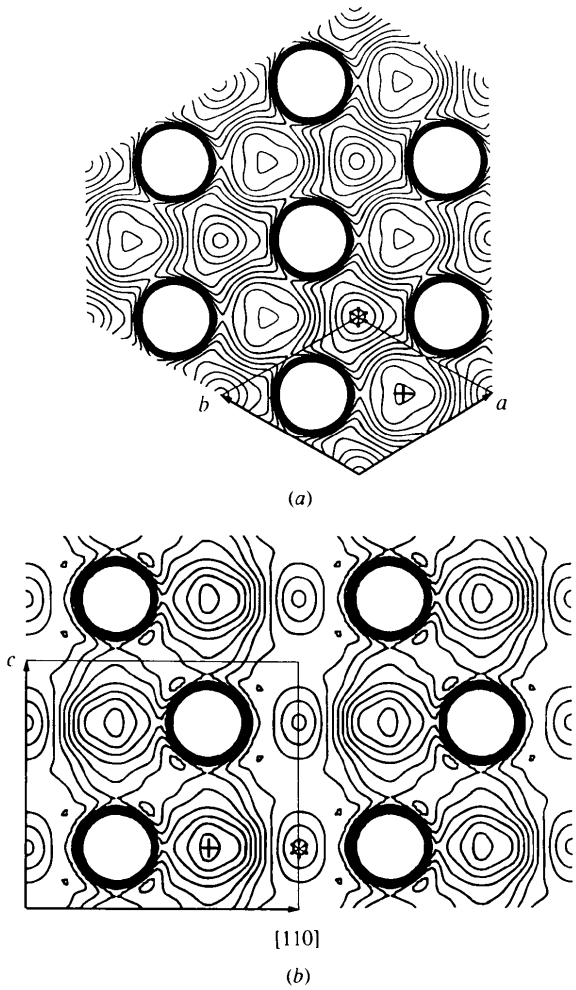

Fig. 1. Contour plots of the MEM electron-density distribution of beryllium based on X-ray single-crystal room-temperature diffraction data. (*a*) shows the basal plane of the h.c.p. structure. The full hexagonal surrounding of one Be atom is displayed. One unit cell is outlined. (*b*) shows the (110) section. More than one unit cell is shown in order to bring out clearly the ABAB stacking along the *c* axis. The maximum density at the atomic position is 48.10 e Å^{-3}. However, the contour plotting was truncated at 0.5 e Å^{-3}. Emphasis is put on the lower density regions of the unit cell by only plotting on a linear scale from 0.0 to 0.5 e Å^{-3} with intervals of 0.025 e Å^{-3}. The density at special position *d*, +, is a local maximum of 0.41 e Å^{-3}, that of special position *b*, *, is a local minimum of 0.14 e Å^{-3} .

In many applications a uniform density is used as prior model. This assumes that we do not know anything about the distribution *a priori* (other than positivity and the total number of electrons). We only make use of the data at hand. We also tried another choice of τ_x, namely the density corresponding to two thermally smeared Be atoms placed at their known position in the unit cell. The rationale behind this distribution is that we make no assumptions of the nature of chemical interactions taking place when forming the crystal. We only assume that matter is made of atoms organized in a h.c.p. lattice. The non-uniform prior distribution of thermally smeared Be atoms was calculated in two steps. A static distribution was obtained using wavefunctions from Clementi & Roetti (1974), and it was calculated and discretized using a modified version of the program *SALLY* (Hansen, 1993). The thermally smeared distribution was obtained by a discrete Fourier transformation of the static density followed by multiplication with a temperature factor obtained in a neutron diffraction study by Larsen, Brown, Lehman & Merisalo (1982), see *Appendix*. The thermally smeared structure factors were then transformed back to direct space. To avoid effects of termination ripples that create negative density regions unsuitable for the MEM procedure, levelling of the density in the interatomic regions was introduced. Any pixel with a value lower than 0.2 e Å^{-3} was given a value of 0.2 e Å^{-3}. The cell was then renormalized to eight electrons, resulting in values of 74.36 e Å^{-3} at the beryllium position and 0.15 e Å^{-3} in the flat background region.

Earlier experiences with the present algorithm have shown that inclusion of many high-order reflections can lead to maps containing 'ghost' features that are physically unreasonable. This has been explained as an effect of inferior quality of the high-order reflections because of, for instance, uncertainty in the corrections for thermal diffuse scattering (Takata, Sakata, Kumazawa, Larsen & Iversen, 1994). Another problem with the present procedure is the observation that the distribution of residual structure factors, $F_H^O - F_H^C$, can be very non-uniform. The error after the optimization is sometimes carried by a few low-order reflections (Jauch & Palmer, 1993). de Vries, Briels & Feil (1993) have proposed a weighting scheme that leads to more uniform residual distributions as well as improved EDD's. Therefore, we introduced a weighting scheme based on standard

Table 1. *The critical-point network of the beryllium h.c.p. structure, as found from topological analysis of the MEM density calculated from a uniform prior and stopping at* $C_1 = 1$

Table entries are: the unit-cell positions in fractional coordinates (x,y,z), special position in space group No. 194 $P6_3/mmc$ (pos), multiplicity of the special position (mult), electron density at the critical point in e Å^{-3} (ρ), Laplacian of the density at the critical point in e Å^{-5} ($\nabla^2\rho$), eigenvalues of the Hessian matrix at the critical point (λ_1, λ_2, λ_3), ellipticity of the bond (ε) and distance to nearest gradient path attractors (R_1,R_2).

	(3,−3) NNM1	(3,−3) NNM2	(3,−1) BOND1	(3,−1) BOND2	(3,−1) BOND3	(3,−1) BOND4	(3,1) RING1	(3,1) RING2	(3,1) RING3	(3,3) CAGE
x	2/3	0	0.507	1/3	0.093	0.144	0	0.075	0.107	0
y	1/3	0	1.013	2/3	0.046	0.288	1/2	0.149	0.554	0
z	1/4	0	1/4	0.054	0.042	0.110	0	0.069	0.094	1/4
pos	*d*	*a*	*h*	*f*	*k*	*k*	*g*	*k*	*k*	*b*
mult	2	2	6	4	12	12	6	12	12	2
ρ	0.408	0.223	0.326	0.275	0.220	0.226	0.264	0.213	0.243	0.143
$\nabla^2\rho$	−2.25	−0.99	0.68	1.95	−0.83	−0.20	−0.30	0.26	3.71	3.30
λ_1	−1.64	−0.69	−1.50	−1.32	−0.52	−0.60	−0.95	−0.31	−0.54	0.54
λ_2	−0.49	−0.21	−1.42	−0.40	−0.47	−0.48	0.18	0.13	1.80	0.96
λ_3	−0.13	−0.09	3.61	3.67	0.16	0.88	0.47	0.44	2.45	1.80
ε			0.05	2.35	0.10	0.24				
R_1			0.69	0.70	1.36	0.90				
			Be	Be	NNM1	Be				
R_2			0.63	1.09	0.24	0.69				
			NNM1	NNM1	NNM2	NNM2				

deviations which were modified by multiplication with the square of the length of the scattering vector of the reflection. As will be shown this leads to more uniform residual distributions and it also proved essential in order to obtain reasonable maps from the non-uniform prior distribution.

Because *MEED* calculates the density on a grid it is necessary to employ an interpolation routine to obtain the density at every point in the unit cell which is needed in the calculation of the topological features. We have employed the Gregory–Newton interpolation scheme (Wylie, 1960). Interpolation in the grid-point experimental density sometimes results in either obscure critical points or the routine will not locate all symmetry equivalent critical points in the cell. The critical points presented in this paper are those that were of stable nature and persisted over a range of values for the constraint C_1 (10 to 0.1). Furthermore, the gradient refined to a value of less than 10^{-4} for these points. The procedures have been implemented in a *FORTRAN* program *CPGRID* (Souhassou, 1993).

Results of the MEM analysis

The critical-point network of the h.c.p. structure

Beryllium has the h.c.p. structure. The critical-point network of the h.c.p. structure was examined by Johnson (1992) using Morse theory. A set of equations sums up properties of the number of critical points in a crystal, N(rank, signature).

(i) $N(3,3) \geq 1$;

(ii) $N(3,1) - N(3,3) \geq 0$;

(iii) $N(3,-1) - N(3,1) + N(3,3) \geq 1$;

(iv) $N(3,-3) + N(3,1) = N(3,-1) + N(3,3)$.

In the case of the h.c.p. structure Johnson was unable to establish a fully attractive network of critical points based solely on Morse theory. He concluded that experimental examination of the critical points is a must to further develop the h.c.p. network. The network he established contradicts experimental observations in one essential way. Special position *d* of the space group $P6_3/mmc$ (the centre of the bipyramidal space) is given as a local minimum, which seems an unlikely suggestion since theoretical and experimental studies of the beryllium structure indicate a charge build up in that area.

Our topological analysis revealed many critical points of all kinds due to the high symmetry of the structure. The number, type and position of the critical points was slightly dependent on the stopping criteria for the iterations and on the prior density. In order to establish the critical-point network of the structure with more certainty we examined densities using a number of constraint values, C_1= 10 , 5, 2, 1, 0.75, 0.5, 0.25, 0.1 and 0.001. Table 1 shows only points that were predominantly present in all maps from C_1 = 10 down to C_1 = 0.1. The values listed in Table 1 refer to the map with C_1 = 1 obtained from a uniform prior distribution.

The dominant interactions in the structure can be illustrated by maps of the gradient paths of the EDD. Fig. 2(*a*) shows the (001) plane and Fig. 2(*b*) the (110) plane. 48 gradient paths are traced backwards from each (3,−3) point. The calculations of the gradient paths are stopped if one of the following criteria are not satisfied: (1) $\rho > 10^{-3}$, (2) $\nabla\rho > 10^{-7}$, (3) the gradient path is more than 0.4 Å from the plotting plane, (4) the gradient path changes its direction by more than 90° between two steps (0.025 Å). Due to criterion (3) many gradient paths vanish close to the NNM and due to the finite number of gradient paths, regions of very flat density appear as extensive white areas on the maps. Fig. 2(*a*), the (001) plane, shows two gradient path attractors, namely the Be atom and one at the non-nuclear maximum at the centre of the bipyramidal space. Gradient paths radiate from the point of coordinates (0,0)

in the basal plane. These three points can be seen as well in Fig. 2(*b*), the (110) plane, which also shows yet another gradient path attractor at (0,0,0), special position *a*. The present *MEED* algorithm calculates the density on a grid. This is computationally heavy and leads to several numerical difficulties when the topological features are subsequently calculated and plotted. It is difficult at this stage to know which critical points are significant. We are dealing with experimental data and error analysis in the MEM is not developed. We firmly believe, based on prior experimental (Larsen & Hansen, 1984) and theoretical (Holzwarth & Zeng, 1994) evidence that the non-nuclear maximum, NNM1 in special position *d*, the centre of two adjacent tetrahedral holes in the h.c.p. structure, is correct. If this is accepted we should find, according to Bader's (1991) theory, bond critical points between the NNM1 and Be. The *CPGRID* program locates two-bond critical points, BOND1 in, and BOND2 between basal planes, and the gradient plots, Fig. 2, support the view that these two-bond critical points between beryllium and NNM1 are not artifacts of the critical-point search on a grid.

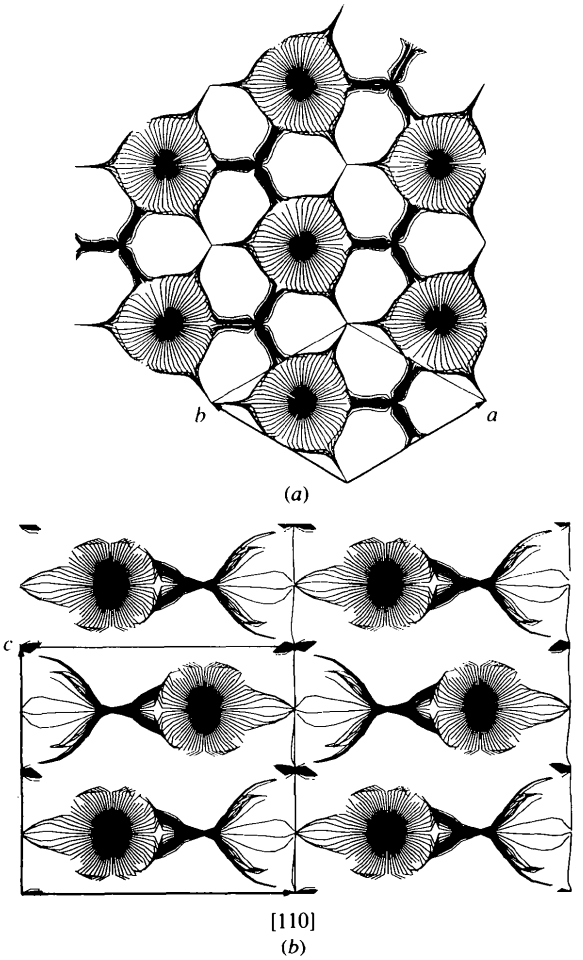

Fig. 2. Gradient paths of the electron-density distribution obtained with the MEM. (*a*) and (*b*) are the (001) and (110) planes, respectively.

The bonds between beryllium and NNM1 outline drum-shaped figures within the h.c.p. structure. The points located in turn demand the existence of ring critical points within four-membered rings consisting of two Be atoms and two NNM1. Ring critical points, RING1, in fact are found in special position *g*, as shown in Table 1. The Morse inequalities also demand at least one cage critical point. To obtain this we accept the second NNM2 which is found in special position *a*, the octahedral hole of the h.c.p. structure. NNM2 is one of the most stable critical points even though this local maximum is found in the low-density region of the structure. Accepting NNM2 we then have the expected cage critical point, CAGE, in special position *b*. However, the presence of NNM2 demands more bond critical points. These are found with perfect octahedral symmetry around NNM2 in special position *k*. There are two different kinds, one, BOND3, connecting NNM1 and NNM2, the other one, BOND4, connecting beryllium and NNM2. These bond paths create a huge number of rings. To fulfil the Morse equations at this stage we need another 24 ring critical points in the cell. This seems to be what we find, namely two different ring critical points, RING2 and RING3, in special position *k*, although they do not fall exactly in the ring planes. The attractive thing about the network at this stage is that the Morse equations are fulfilled. The *CPGRID* program actually locates another three critical points in *k* special positions, two local minima and one local maximum. They are of low density. Accepting these would break the Morse equations and furthermore, the positions of these points are not obviously meaningful. A very essential critical point, namely NNM1, changed character as C_1 was lowered. When reaching $C_1 = 0.5$, this critical point splits up in two symmetrical critical points above and below the basal plane. These two new NNM have a (3,–1) bond critical point in between them at the basal plane position. This splitting of the basal plane NMM indicates that the data suggest a very flat density in this region of the structure. Fig. 3 presents our suggestion of a possible network of critical points for the beryllium h.c.p. structure.

The possibility for including prior knowledge about the system being studied is a strong point in the MEM. The introduction of a prior density consisting of two thermally smeared Be atoms proved to be less satisfactory than the uniform prior distribution, but still very informative. The starting constraint value with this distribution is $C_1 = 31\,480$ compared with 149 549 for the uniform distribution. With this prior distribution convergence is quickly reached, but the corresponding map is full of spurious features. The topological analysis revealed only few critical points at special positions. It seems that the *MEED* algorithm does not provide a physically meaningful answer if the thermally smeared atomic density is chosen as prior. Maybe the thermally smeared atomic prior introduces bias against moving

Table 2. *Relative residuals,* $(F^o - F^c)/\sum(F^o - F^c)$ *in %, for selected low-order reflections using different prior distributions and weighting schemes in the MEM*

The two first columns show the MEM results obtained with a uniform prior distribution and weights $1/\sigma^2$, $1/(H^2\sigma)^2$. The following two columns show the results obtained using a thermally smeared free atom Be distribution with $1/\sigma^2$, $1/(H^2\sigma)^2$ weights, respectively.

	Uniform prior	Uniform prior	Non-uniform prior	Non-uniform prior	
h,k,l	$w = 1/\sigma^2$	$w = 1/(H^2\sigma)^2$	$w = 1/\sigma^2$	$w = 1/(H^2\sigma)^2$	$\lvert F_H^o \rvert$
1,0,0	3.69	0.33	9.39	0.79	1.852
0,0,2	8.09	0.41	0.77	2.92	3.371
1,0,1	51.59	3.05	33.59	4.25	2.835
1,0,2	4.91	2.28	2.61	0.32	1.483
1,1,0	4.34	9.29	14.01	15.86	2.687
1,0,3	6.81	21.74	10.28	15.44	2.166
2,0,0	1.78	1.89	2.15	0.64	1.197
1,1,2	9.72	29.07	12.36	17.45	2.352
2,0,1	1.84	19.88	6.45	11.14	2.021
0,0,4	2.08	2.13	3.98	2.09	2.232
2,0,2	2.77	0.56	1.19	3.36	1.051
1,0,4	1.40	1.39	1.58	0.98	1.002
2,0,3	0.30	1.45	0.47	0.86	1.561
2,1,0	0.06	0.30	0.05	0.22	0.869
2,1,1	0.30	1.12	0.44	1.20	1.459
1,1,4	0.06	0.65	0.15	0.96	1.617
2,1,2	0.03	0.12	0.02	0.05	0.768
1,0,5	0.09	0.59	0.05	0.83	1.316
$\Sigma\Delta$	0.336	0.338	0.405	0.407	—
R-factor	0.00592	0.00594	0.00711	0.00715	—

density into the interatomic region compared with the uniform prior which is the least biased prior. Jauch & Palmer (1993) also examined the influence of non-uniform priors. They found the low-density regions to be strongly affected by the choice of prior, whereas the peaks were almost unaffected. In our case the high-density regions are also affected by the choice of prior. The peak value at the beryllium position at C_1 = 1 for the thermally smeared beryllium prior is 53.5 e Å^{-3}, compared with 48.1 e Å^{-3} for the uniform prior. This is a demonstration of the point stated earlier, namely that two distributions with almost identical misfit statistics can be quite different.

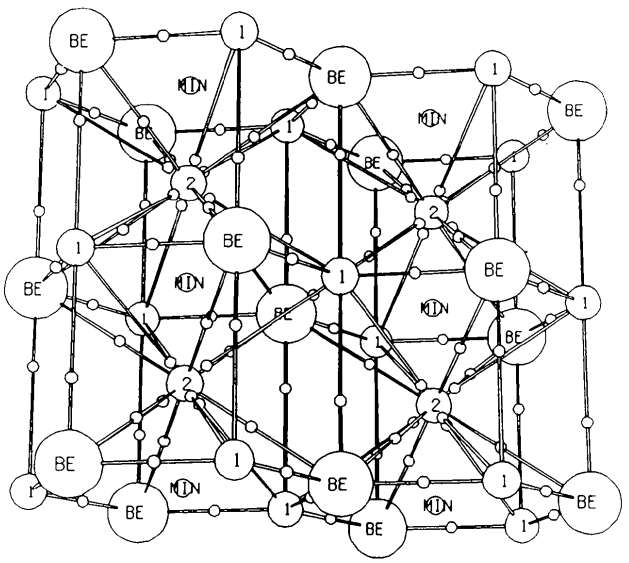

Fig. 3. Possible critical-point network for the beryllium h.c.p. structure obtained from the topological analysis of the MEM electron-density distribution. The non-nuclear maxima NNM1 and NNM2 are marked 1 and 2, respectively. The CAGE point is marked MIN.

Introduction of a weighting scheme changes the MEM maps considerably when the prior density consists of two thermally smeared Be atoms. Putting less weight on the high-order reflections allow the optimization procedure to assemble more charge in the valence regions and an increased charge build up is observed around the bipyramidal space of tetrahedral holes. Multiplication by H^2 on the standard deviations, H being the length of the scattering vector, clearly establishes the NNM1. With the H^2 weighting the NNM2 is not present as a (3,–3) but as a (3,–1) critical point. The overall tendency is for the maps to become much more symmetric, and ghost features disappear when putting extra weight on the low-order reflections. In the present context the important thing is that we can retrieve non-nuclear maxima in the EDD of metallic beryllium starting from priors 'from both sides' of the final map. This strongly supports their presence. We also introduced the same weighting of the reflections in calculations with the uniform prior. The resulting maps are very similar to those obtained without weighting. The charge build up in the bipyramidal region is still dominant and the overall features with two NNM interconnected with beryllium through (3,–1) critical points are still present after the weighting.

Jauch & Palmer (1993) observed that the distribution of residual structure factors, $F_H^O - F_H^C$, after a MEM procedure was quite non-uniform. Most of the error was carried by a few low-order reflections, whereas the high-order reflections are reproduced almost perfectly. Table 2 shows relative errors in per cent for the low-order reflections for different choices of prior distribution and weighting. As can be seen, introduction of the H^2 weighting scheme results in a more uniform scatter of the residuals.

Table 3. *Final parameters and residuals for the multipole refinements*

Model 2 employs thermal parameters determined by least-squares refinement of neutron data (Larsen, Brown, Lehman & Merisalo, 1982) using a Gram–Charlier expansion to fourth order of the harmonic displacement factor (see *Appendix*). The values in the table are related with the parameters in the temperature-factor expression, (4) by C^{jkl} (Table 3) $= C^{jkl} \times 4/3\pi^3 \times a_j^* a_k^* a_l^*$ and D^{jklm} (Table 3) $= D^{jklm} \times 2/3\pi^4 \times a_j^* a_k^* a_l^* a_m^*$.

	Model 1	Model 2
Scale	0.992 (4)	0.991 (2)
U^{11} (Å^{-2})	0.00599 (14)	0.00587*
U^{33} (Å^{-2})	0.00520 (14)	0.00536*
C^{111} (Å^{-3})	0.0015 (4)	0.00228*
D^{1111} (Å^{-4})	−0.00002 (31)	−0.00011*
D^{3333} (Å^{-4})	−0.0002 (4)	−0.00020*
D^{1133} (Å^{-4})	−0.0006 (62)	0.00069*
P_{00}	2.0	2.0
P_{20}	−0.0015 (54)	−0.13 (10)
P_{33+}	0.073 (37)	0.15 (7)
P_{40}	0.013 (78)	−0.14 (15)
k'	0.862 (20)	0.846 (25)
k''	1.0*	1.0*
ζ	1.0*	1.0*
R_F	0.0033	0.0061
R_{wF}	0.0032	0.0069
R_F^2	0.0081	0.0133
R_{wF}^2	0.0065	0.0137
Gof	0.987	1.973

* Not refined.

Results of the MRM analysis

To compare with the findings of the MEM, multipole refinements were carried out with the same set of structure factors using the program *MOLLY* (Hansen & Coppens, 1978), and subsequently the topology of the corresponding EDD was analysed. The atomic density was expanded to hexadecapole level. Be atoms have site symmetry $\bar{6}m2$ and, therefore, only three multipoles are allowed up to fourth order, namely P_{20}, P_{33+} and P_{40}. The topological analysis of the resulting static densities was carried out with the program *POTLAPDENS* (Souhassou, 1993). The electron density calculated using the MRM is dependent on the model used to fit the data. A first model, model 1, contained atomic scattering functions centred at the beryllium position. The model also included Gram Charlier expansion parameters of the temperature factor $T(\mathbf{H})$ (4), up to fourth order for describing the anharmonic vibrations of the beryllium nuclei.

$$T(\mathbf{H}) = (1 - 4i\pi^3/3C^{jkl}h_jh_kh_l + 2\pi^4/3D^{jklm}h_jh_kh_lh_m)\, T_{\text{harmonic}}(\mathbf{H}), \quad (4)$$

with

$$T_{\text{harmonic}}(\mathbf{H}) = \exp(-P^{ij}h_ih_j).$$

Even though metallic beryllium is an extremely hard material (Debye temperature = 1150 K), it has been shown (Larsen, Brown, Lehman & Merisalo, 1982; Takata, Sakata, Kumazawa, Larsen & Iversen, 1994) that even at room temperature significant third- and fourth-order contributions are present in the anharmonic motion of beryllium. We have adopted the axis definitions: [001] along the $\bar{6}$ axis, and [120] along the 2 axis. The following symmetry restrictions on the contravariant thermal parameters then apply (*International Tables for Crystallography*, 1974).

Second order: $P^{11} = P^{22} = 2P^{12}$, P^{33}

Third order: $C^{111} = -C^{222} = 2C^{112} = -2C^{122}$

Fourth order: $D^{1111} = D^{2222} = 2D^{1112} = 2D^{1222} = 2D^{1122}$, $D^{1133} = D^{2233} = 2D^{1233}$, D^{3333}.

All other thermal parameters are zero. Results from the least-squares refinement of model 1 are given in Table 3.

Figgis, Iversen, Larsen & Reynolds (1993) found in their study of copper Tutton's salt, that unbiased neutron parameters can be vital in electron-density modelling using the multipole technique. In order to extract the optimum amount of electronic information about the system, presumably unbiased thermal parameters were therefore first obtained by least-squares refinement of the neutron diffraction data of Larsen, Brown, Lehman & Merisalo (1982) (see *Appendix*). These thermal parameters were used as fixed values in a second model in the MRM analysis. Final parameters for model 2 are also given in Table 3.

Static deformation maps of model 2 are given in Fig. 4. In the region around the bipyramidal space they show an excess of charge relative to a procrystal consisting of spherical Be atoms. Topological analysis of the static density reveals that model 2 contains NNM1 but not NNM2 found in the MEM case. The bond critical point, BOND1, and the cage critical point, CAGE, are also present. No bond critical point is found between beryllium and NNM1 of adjacent (001) layers. Instead a (3,3) cage critical point is found between them. However, for this point two eigenvalues are very small ($\lambda_1 = \lambda_2 = 0.06$). It will only take a minor change in the EDD to change the topology of this point and make it a (3,−1) bond critical point like BOND2 of the MEM case. Several spurious ring critical points are indicated but none in special positions. The critical points are listed in Table 4. Maps of the gradient paths corresponding to the static EDD of model 2 are shown in Fig. 5, which appears rather different from Fig. 2, the gradient maps of the MEM EDD. The volumes around the Be atoms though are quite similar. The absence of NNM2 in the static MRM EDD is matched by pronounced differences between the gradient paths in the interatomic region.

In order to test the resolution which is attainable without use of unbiased neutron parameters, we have also performed a topological analysis of the static density corresponding to model 1. It is satisfying to observe that model 1 contains the NNM1. It also contains both of the (3,−1) bond critical points between beryllium and NNM1 found with the MEM. Model 1 indicates additional (3,−1) points plus another NNM, which are all in general positions and seem to be spurious. The density

Table 4. *Values at selected critical points in the EDD obtained with the MRM using model 2*

Table entries correspond to the entries of Table 1.

	(3,−3) NNM1	(3,−1) BOND1	(3,3) CAGE (BOND2)	(3,3) CAGE
x	2/3	0.481	1/3	0
y	1/3	0.519	2/3	0
z	1/4	1/4	−0.050	1/4
pos	*d*	*h*	*f*	*b*
mult	2	6	4	2
ρ	0.382	0.350	0.288	0.232
$\nabla^2\rho$	−0.77	0.62	1.64	0.91
λ_1	−0.24	−0.65	0.06	0.44
λ_2	−0.29	−0.40	0.06	0.44
λ_3	−0.24	1.66	1.99	0.03
ε		0.63		
R_1		0.59 Be	1.05 Be	
R_2		0.73 NNM	0.74 NNM	

distribution of model 1 is more noisy than what is found for model 2. The general topology of the MRM models, however, resembles what is found with the MEM. The most important difference in the topology between the MEM and the MRM model is the presence of NNM2 in the MEM density. Compared with the MEM the MRM has resulted in the more noisy EDD, and thus for the beryllium structure it seems that extremely fine details in the EDD are better revealed by the MEM.

Discussion

The critical bond network of bulk beryllium shown in Fig. 3 is complex and suggests some special properties of the bonding in metallic Be. It is interesting to compare the characteristics of the critical points with those found in lithium. In lithium bonds between the metal atoms and the NNM can be characterized as closed-shell interactions ($\nabla^2\rho > 0$). This is also the case for the two bond critical points between NNM1 and Be.

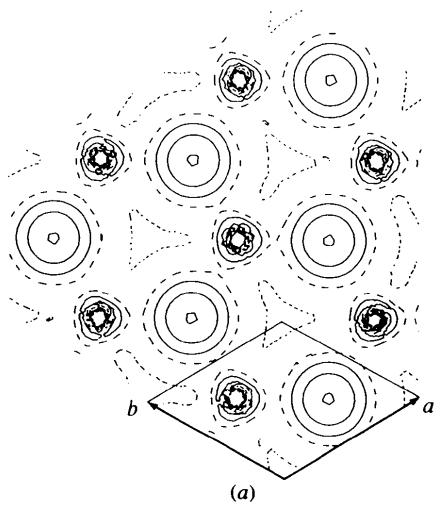

(*a*)

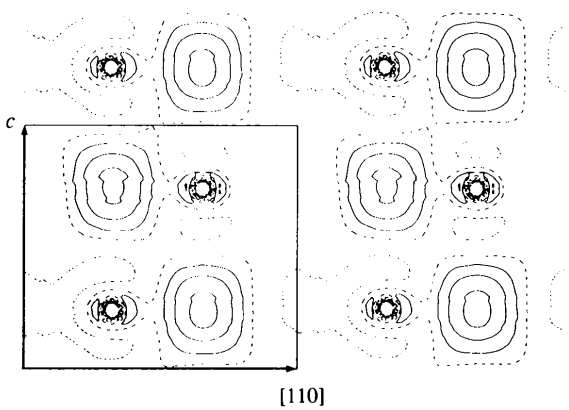

[110]

(*b*)

Fig. 4. Static deformation densities for the multipole least-squares analysis based on model 2. (*a*) and (*b*) are the (001) and (110) planes, respectively. Contour interval = 0.02 e Å^{-3}. The static density is calculated from a 93 unit-cell model density.

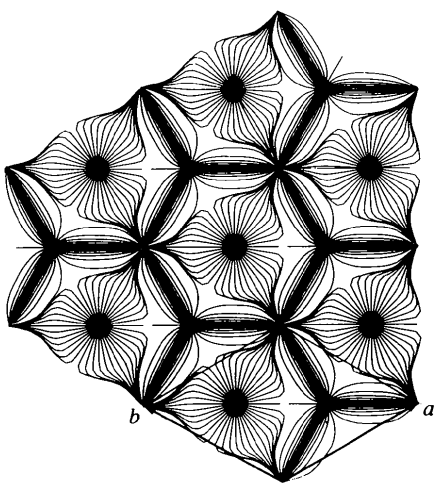

(*a*)

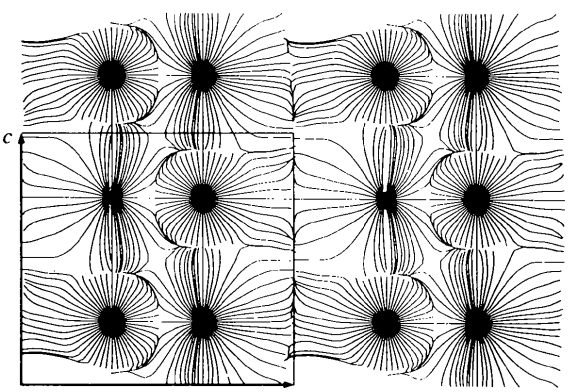

[110]

(*b*)

Fig. 5. Gradient paths of the electron-density distribution obtained from the multipole analysis. (*a*) and (*b*) are the (001) and (110) planes, respectively.

However, both the (3,–1) point between beryllium and NNM2 and the (3,–1) point between the two NNM have negative Laplacians. These bonds can therefore be characterized as shared interactions. A negative value of the Laplacian indicates a surplus of potential energy density relative to kinetic energy density. Regions of negative Laplacians are also found at the position of the beryllium nuclei and at the two NNM. This indicates that the two NNM sit in positions that are optimally stabilized by a large number of surrounding beryllium nuclei. NNM1 has three beryllium neighbours at short distance and two more at longer distances limiting the bipyramidal space. Part of the bonding in metallic beryllium may therefore be viewed as a five-centre bond. NNM2 has six beryllium nuclei as neighbours but at a somewhat larger distance.

The topological analysis reveals a picture that differs from the simple qualitative picture obtained by Takata, Kubota & Sakata (1993) from synchrotron powder diffraction data. Based on recognition of the regions of maximally accumulated charge they concluded that the charge in the bipyramidal space binds the atoms within one layer but that there is no overlap of electrons between planes. In this way they argued that beryllium has an electronic layer structure. The critical-point network in Fig. 3 opposes this view of the beryllium structure. The topology suggests inter-layer interactions. The layer atoms are bound to each other through the NNM1. The existence of NNM2 spoils the layer picture. With the NNM2 present we establish the inter-meshed network of negatively charged pseudo-atoms like that proposed by Cao, Gatti, Macdougall & Bader (1987) for the group I metals. Bader (1991) argues that the charge in pseudo-atoms should be mobile under the influence of an electric field and primarily responsible for the conducting properties of the metal. The structure in Fig. 3 has a multitude of zigzag channels formed by the pseudo-atom network in which conduction can occur.

The topological network may be able to explain some of the abnormal surface effects that have been observed for Be. Surface reorganization has attracted considerable theoretical and experimental interest in recent years due to surface critical, modern technology. At the surface the atomic positions that minimize the free energy for the bulk structure do not necessarily minimize the free energy at the surface. In some cases the surface reconstructs, but in less extreme cases the lattice near the surface is relaxed. The interesting point is that beryllium has an abnormally large expansion of the lattice at the surface. This is opposite to the majority of close-packed crystal structures which show contractions or at the most small expansions. This abnormal behaviour is expected to lead to interesting physical and chemical properties of the beryllium surface. Boettger & Trickey (1985) reported density functional calculations showing that bilayers of beryllium expand the *c/a* ratio to 1.69 compared with 1.56 in the bulk. The increase of the *c/a* ratio is due to both in-layer contraction and inter-layer expansion. Davis, Hannon, Ray & Plummer (1992) have recently determined surface inter-layer distances from LEED spectra of the (001) surface. They report that the surface layers have an abnormally large expansion of 5.8%. The abnormal effects at the beryllium surface fits into our topological picture of the bulk with important inter-layer interactions. When the surface is created, the network comprising the pseudo-atoms is disturbed, leading to a weakening of the inter-layer bonding near the surface which in turn results in the expansion of the inter-layer distance. The electrons that in the bulk make up the inter-layer overlap may at the surface reorganize into the plane resulting in the in-plane contraction. It is notable that beryllium has a *c/a* less than the ideal 1.63, in support of the idea of inter-layer interactions in Be. If these observations are correct then it will have some implications for h.c.p. metals with $c/a > 1.63$. They should show weaker inter-layer interactions in the bulk. We are presently carrying out a similar topological analysis for magnesium to explore these ideas.

Table 5. *Atomic charges in spherical volumes calculated using results of the MEM with different prior distributions and weighting schemes*

Column 5 corresponds to the thermally smeared free atom Be starting distribution used as prior distribution in the MEM calculation with non-uniform prior.

Radius of spherical volume (Å)	Uniform prior $w = 1/\sigma^2$	Non-uniform prior $w = 1/\sigma^2$	Non-uniform prior $w = 1/(H^2\sigma)^2$	Thermally smeared free atom Be distribution
Be, $R = 0.69$	2.32	2.45	2.40	3.04
Be, $R = 0.90$	2.88	2.98	2.93	3.36
NNM1, $R = 0.63$	0.48	0.36	0.41	0.26
NNM2, $R = 0.24$	0.02	0.02	0.01	0.01
NNM2, $R = 0.69$	0.40	0.43	0.42	0.27

The topological analysis indicates that the volume associated with the Be atom can be quite well approximated by a spherical volume. Beryllium has three-bond critical points at distances 0.69, 0.70 and 0.90 Å, respectively. Integration over a sphere with such radii reveals the charges given in Table 5. Table 5 shows the results obtained with the MEM, starting with both a uniform and a non-uniform prior. Furthermore, the charges corresponding to the thermally smeared beryllium density which was used as a starting distribution in the non-uniform MEM procedure, are given. It is clear that charge has moved into the bipyramidal region during the optimization and the numbers suggest that the Be atom in the metal is stripped of most of its valence electrons and consists primarily of an ionic core. The valence electron density is primarily found near the non-nuclear maxima. NNM1 has neighbouring bond critical points at 0.63, 1.09 and 1.36 Å. Results obtained by integration over a sphere of radius 0.63 Å are shown in Table 5. This lower estimate is probably a considerable underestimate of the NNM1 charge, because the NNM1

basin is highly non-spherical. The average density in the unit cell outside the Be atoms (spheres of radii 0.9 Å) is 0.182 e Å^{-3}. A spherical NNM1 of radius 0.63 Å has an average density of 0.356 e Å^{-3}. NNM2 has neighbouring (3,–1) points at 0.24 and 0.69 Å and integration results are also shown in Table 5. The average density for an NNM2 sphere of radius 0.24 Å is 0.218 e Å^{-3}.

Concluding remarks

In the combined process of deriving the EDD by the MEM and subsequent topological analysis a detailed description of the beryllium structure has been achieved without using any model. The proposed critical-point network should be interpreted with care, keeping in mind the uncertainties in the present procedures. However, the network gives some explanation for the well established abnormal behaviour of the beryllium surface.

The MEM results were compared with results from the MRM. The MRM is a very well established technique and for molecular crystals it is probably at the present stage superior to the MEM. However, the MRM formalism lacks a measure besides the χ^2 statistic for judging the validity of different models. Some kind of prior distribution should be incorporated to measure the entropy of the derived distribution. The EDD's obtained with the MRM confirm the general topological features from the MEM, but the fine details are less clear. It is satisfying that both methods independently reveal that non-nuclear maxima exist in the EDD of the beryllium h.c.p. structure.

The problem with the MEM is that it is computationally heavy. In the present form it uses a discrete density which creates some numerical difficulties and there are some problems in the method that are still unresolved. The problem with the stopping criteria has to be further addressed to make the method consistent and the effects of the different weighting schemes and prior densities must be better understood. Perhaps additional constraints should be included when we are stretching the experimental resolution to the limit. There may be, for example, correlations between neighbouring pixels as we are dealing with a system of Fermi ions. A limitation in the present method is that it demands use of data virtually free of systematic errors, which are difficult to obtain except in a few specific cases like beryllium. However, the MEM is a powerful method which is model independent, and the present study shows that inclusion of the prior distribution can make a difference.

The authors wish to thank Professor N. K. Hansen for his kind assistance with the MRM calculations. This work has been partly supported by the Danish Natural Science Research Council, the American National Institutes of Health and by the Ministry of Education, Science and Culture of Japan.

Table 6. *Results of least-squares refinement of neutron data*

Parameter	Value
No. of observations	132
Scale	55.4 (1)
U^{11} (Å^{-2})	0.00587 (4)
U^{33} (Å^{-2})	0.00536 (4)
C^{111} (Å^{-3})	0.00227 (36)
D^{1111} (Å^{-4})	−0.00011 (4)
D^{3333} (Å^{-4})	−0.00020 (5)
D^{1133} (Å^{-4})	−0.00069 (13)
ε (isotropic extinction)	0.009 (2)
R_F	0.0075
R_{wF}	0.0103
R_{F^2}	0.0129
R_{wF^2}	0.0206
Gof	0.694

APPENDIX

Results of least-squares refinement of neutron data (see Table 6)

The refinement of the neutron data (Larsen, Brown, Lehman & Merisalo, 1982) was done with the program *MOLLY* (Hansen & Coppens, 1978) employing the Gram Charlier expansion up to fourth order of the harmonic displacement factor. In accordance with Larsen, Brown, Lehman & Merisalo (1982) and Takata, Sakata, Kumazawa, Larsen & Iversen (1994), we find both significant third- and fourth-order anharmonicity. It is of interest to compare the values of the thermal parameters obtained from the neutron data with the parameters obtained from the X-ray data (model 1). Especially the important third-order parameter C^{111} is more significant in the neutron study. This parameter correlates with the third-order multipole P^{33+} in the X-ray refinements. The P^{33+} multipole is primarily responsible for moving charge out into the bipyramidal region. A significant value of C^{111} indicates that the atomic potentials are softened towards the side which is part of the rectangular configuration of the neighbouring atoms and hardened against the direction of the bipyramidal space. The third-order anharmonicity and the electron deformation thus have opposite effects. When the unbiased neutron parameters are used the value of P^{33+} increases from 0.073 to 0.152. The result of this is seen in the static deformation maps of model 2, where a large peak at the position of NNM1 indicates that the beryllium structure contains more charge in this region than a procrystal consisting of free Be atoms placed at their unit-cell positions.

References

BADER, R. F. W. (1991). *Atoms in Molecules. A Quantum Theory*. Oxford Univ. Press.

BOETTGER, J. C. & TRICKEY, S. B. (1985). *Phys. Rev. B*, **32**, 1356–1358.

CAO, W. C., GATTI, C., MACDOUGALL, P. J. & BADER, R. F. W. (1987). *Chem. Phys. Lett.* **141**, 380–385.

CHOU, M. Y., LAM, P. K. & COHEN, M. L. (1983). *Phys. Rev. B*, **28**, 4179–4185.

CLEMENTI, E. & ROETTI, C. (1974). *At. Data Nucl. Tables*, **14**, 177–478.

COLLINS, D. M. (1982). *Nature (London)*, **298**, 49–51.

DAVIS, H. L., HANNON, J. B., RAY, K. B. & PLUMMER, E. W. (1992). *Phys. Rev. Lett.* **68**, 2632–2635.

DOVESI, R., PISANI, C., RICCA, F. & ROETTI, C. (1982). *Phys. Rev. B*, **25**, 3731–3739.

EDGECOMBE, K. E., SMITH, V. H. & MULLER-PLATHE, F. (1993). *Z. Naturforsch. Teil A*, **48**, 127–133.

FIGGIS, B. N., IVERSEN, B. B., LARSEN, F. K. & REYNOLDS, P. A. (1993). *Acta Cryst.* B**49**, 794–806.

GULL, S. F. (1989). In *Maximum Entropy and Bayesian Methods*, edited by J. SKILLING, pp. 53–71. Dordrecht: Kluwer Academic Press.

HANSEN, N. K. (1993). *SALLY*. Laboratoire de Mineralogie et Cristallographie, Univ. de Nancy I, BP 239, 54506 Vandoeuvre CEDEX, France.

HANSEN, N. K. & COPPENS, P. (1978). *Acta Cryst.* A**34**, 909–921.

HOLZWARTH, N. A. W. & ZENG, Y. (1994). *Phys. Rev. B.* Submitted.

JAUCH, W. & PALMER, A. (1993). *Acta Cryst.* A**49**, 590–591.

JOHNSON, C. K. (1992). Am. Crystallogr. Assoc. Annu. Meet., Univ. of Pittsburgh. Abstract PA99, 105.

KAPUR, J. N. & KESAVAN, H. K. (1992). *Entropy Optimization Principles with Applications*. New York: Academic Press.

KUMAZAWA, S., KUBOTA, Y., TAKATA, M., SAKATA, M. & ISHIBASHI, Y (1993). *J. Appl. Cryst.* **26**, 453–457.

LARSEN, F. K. & HANSEN, N. K. (1984). *Acta Cryst.* B**40**, 169–179.

LARSEN, F. K., BROWN, P. J., LEHMAN, M. S. & MERISALO, M. (1982). *Philos. Mag. B*, **45**, 31–50.

ROSS, R. B., ERMLER, W. C., KERN, C. W. & PITZLER, R. M. (1992). *Int. J. Quantum Chem.* **41**, 733–747.

SAKATA, M. & SATO, M. (1990). *Acta Cryst.* A**46**, 263–270

SKILLING, J. (1989). In *Maximum Entropy and Bayesian Methods*, edited by J. SKILLING, pp. 46–53. Dordrecht: Kluwer Academic Press.

SKILLING, J. (1991). *Maximum Entropy in Action*, edited by B. BUCK & V. A. MACAULAY, pp. 19–40, Oxford: Clarendon Press.

SMITH, C. R. & ERICKSON, G.(1989). In *Maximum Entropy and Bayesian Methods*, edited by J. SKILLING, pp. 29–44. Dordrecht: Kluwer Academic Press.

SOUHASSOU, M. (1993). *CPGRID* and *POTLAPDENS*. Laboratoire de Mineralogie et Cristallographie, Univ. de Nancy I, BP 239, 54506 Vandoeuvre CEDEX, France.

STEWART, R. F. (1976). *Acta Cryst.* A**32**, 565–574.

STEWART, R. F. (1977). *Acta Cryst.* A**33**, 33–38.

STEWART, R. F. (1991). In *The Application of Charge Density Research to Chemistry and Drug Design*, NATO ASI Ser. B., Vol. 250. New York: Plenum Press.

TAKATA, M., SAKATA, M., KUMAZAWA, S., LARSEN, F. K. & IVERSEN, B. B. (1994). *Acta Cryst.* A**50**, 330–337.

TAKATA, M., KUBOTA, Y. & SAKATA, M. (1993). *Z. Naturforsch. Teil A*, **48**, 75–80.

VRIES, R. Y. DE, BRIELS, W. J. & FEIL, D. (1993). *Acta Cryst.* A**50**, 383–391.

WYLIE, C. R. (1960). *Advanced Engineering Mathematics*, 2nd ed. New York: McGraw-Hill.